Effects of Tool Tilt Angle and Plunge Depth on Properties of Polycarbonate FSW Joint

Hamidreza Mohammadi Kuhbanani[1], Hesameddin Yasemi[1], Hamed Aghajani Derazkola[2*]

[1]Shahid Dadbin Technical and Vocational University, Kerman, Iran
[2]Young Researchers and Elites Club, Science and Research Branch, Islamic Azad University, Tehran, Iran
[*]Email of Corresponding Author: hamed.aghajani@srbiau.ac.ir

Abstract
In the present article, the effects of friction stir welding (FSW) tool plunge depth (TPD) and tool tilt angle (TTA) were investigated on the heat generation and the material flow during solid-state joining of polycarbonate (PC) sheet experimentally and simulated with computational fluid dynamics (CFD) method. Simulation results showed that increasing heat input (higher TTA and lower TPD) could increase the size of the stir zone. Results indicate that control of TPD and TTA can improve the material flow near the top surface. The temperature field in the friction stir welding of PC was anti symmetric to the welding line. Due to the results, the heat generation and temperature distribution at the advancing side were more than the retreating side in all joint conditions. According to selected parameters, a strong sample was produced at 1.2 TPD and 2.5 oTTA. This sample had 92% PC tensile strength, 89% PC flexural strength, and 86% of impact energy.

Keywords

1. Introduction
Thermoplastic polymers and their composites are widely employed. In many applications, they replaced metallic materials. This is due to lower material cost, easier and less expensive processing, recyclability, etc. Besides, thermoplastics with high strength to weight ratios are increasingly involved in structural applications. The growing employment and development of new materials are also driven by the spread of Additive Manufacturing processes. The selection of the suitable joining process represents a key aspect for the manufacturing of real components. Common joining techniques e.g. adhesive bonding, mechanical fastening, and even welding processes show different disadvantages and limitations. To this end, advanced welding and joining processes such as laser welding, laser-assisted joining friction stir welding, etc. provide great advantages over common joining processes [1–4]. Friction Stir Welding (FSW) is used to join different materials including metals, thermoplastics, composites and hybrid structures [5-8]. FSW enables great homogeneity of the composition of the weld region with the base material, few internal defects, great process efficiency, and high flexibility. FSW process consists of the stirring action of two sheets exerted by a rotating tool. This makes FSW also suitable for joining most of the thermoplastic materials [9-10]. The literature concerning FSW of metals and especially aluminum alloys is extremely wide, while investigations concerning FSW of polymers are much fewer. Besides, the FSW of polymers (semi-

solid welding) develops quite differently from the FSW of metals (solid-state welding). This is due to the great difference between these materials in terms of mechanical and thermal properties, chemical and physical behaviors. In recent years, the wider employment of thermoplastics polymers and their composites for structural and high-performing applications is driving towards a renewed interest in FSW of polymers and composites. FSW has been applied to a wide range of thermoplastics. The influence of process parameters on the mechanical behavior of FSW welds made on polyethylene (PE) was investigated in [11]. Subsequent research demonstrated that pre-heating of the base material can improve the material flow and consequently the FSW quality. The adoption of low tool rotation speed produced some defects in the stir zone (SZ), which affected the mechanical strength of HDPE welds. This was due to a poor stirring action [12]. On the other hand, extremely high tool rotation speed can cause degradation phenomena and even polymer burning. Saeedy and Givi [13] performed the optimization of the FSW process of HDPE sheets. The welds performed under optimal conditions reached strength of 75% of that of the base material. As the process is based on the stirring action exerted by the tool on the sheets, the geometry dimension and topology of the tool also represents a key aspect for the quality of FSW welds. For example, a tool with a threaded pin can reduce cavities and inclusions in the stir zone as well as improve the consolidation of polypropylene (PP) sheets [14]. When threaded tools are used, the tool rotation direction influences the quality of the welds, as described by Panneerselvam and Lenin [15] for polyamide 6. The results indicated that clockwise rotation improved the strength of the welds and internal material flow. Based on the similarity with the extrusion welding process, some researches involved a stationary shoulder (called "shoe") to improve the FSW quality of PE joints. FSW has been applied to polymers characterized by very different behaviors e.g. brittle materials such as Polymethylmethacrylate (PMMA) and plastic materials such as Polycarbonate (PC). Polymethylmethacrylate (PMMA) is widely used in different fields. Simões and Rodrigues investigated the thermos-mechanical conditions developing during the FSW of PMMA [16-17]. Investigation of the effects of FSW process parameters on the PMMA joint showed the highest strength. The longitudinal tensile sample of the PMMA lap joint was 64% and the traverse tensile sample was 47% of base material strength. Although Polycarbonate (PC) is more expensive than PMMA, it is often preferred when high mechanical, toughness, and corrosion properties are required. Thus, some researches focused on friction stir spot welding (FSSW) of PC sheets. During the mentioned researches, mechanical properties, control of plunging force, analysis of temperature, effects of tool shoulder diameter and angle of tool pin were investigated [18]. Low values of the plunging speed involved lower plunging force and torque. However, these conditions affected the mechanical behavior of the FSSW welds. The results from the above-mentioned researches indicated that the most influencing parameters for the joint strength and weld extension were the FSSW tool plunge rate, the tool dwell, and the waiting time. On the other hand, the pin diameter influenced the process loads and the axial pressure [19]. So far, few investigations were performed on continuous FSW of PC. This study aims to investigate the effects of FSW process parameters (tool rotational speed, tool traveling speed, tool tilt angle, and tool plunge depth) on the mechanical properties and material flow of PC welds made by FSW. To this end, both the experimental approach and numerical modeling were involved to understand material behavior during the welding process.

2. Process Modeling

2.1. Governing Equations

The computational domain in this study includes the workpiece and the tool inserted inside the workpiece. During the simulation tool, the plunge stage and extraction from the joint line are neglected for simplicity. Therefore, the temperature and velocity fields are solved assuming steady-state behavior. The plastic flow in a three dimensional space is represented by the momentum conservation equation in index notation, with i or j = 1, 2 and 3, representing x, y and z directions, respectively [19-20]:

$$\rho\frac{\partial u_i u_j}{\partial x_i} = -\frac{\partial P}{\partial x_j} + \frac{\partial}{\partial x_i}\left(\mu\frac{\partial u_i}{\partial x_j} + \mu\frac{\partial u_j}{\partial x_i}\right) - \rho U_1\frac{\partial u_j}{\partial x_1} \tag{1}$$

In Equation (1), u is the velocity, ρ is the density, U1 is the welding velocity, and P is the pressure. μ is referring to non-Newtonian viscosity that can be determined from flow stress and effective strain rate as follows [21-23]:

$$\mu = \frac{\sigma_e}{3\dot{\varepsilon}} \tag{2}$$

The calculation of viscosity requires a local value of strain rate and temperature. In Equation (2), σ_e indicated the flow stress that proposed by Sheppard and Wright [21-23]:

$$\sigma_e = \frac{1}{\alpha}arc\sinh\left(\frac{Z}{A}\right)^{\frac{1}{n}} \tag{3}$$

Where A, a and n are material constants and Z is the Zener–Hollomon parameter. The value of constants for AA1100 aluminum alloy are A = 3.51 $*10^{10}$ S^{-1}, a=1 MPa^{-1}, and n=5.66 [17]. The Zener–Hollomon parameter, Z, represents the temperature compensated effective strain rate and is given by [21-23]:

$$Z = \dot{\varepsilon}exp^{\left(\frac{Q}{RT}\right)} \tag{4}$$

Where Q=158.3kJ/mol is the temperature-independent activation energy, R is the universal gas constant, $\dot{\varepsilon}$ is the effective strain rate and given by [23]:

$$\dot{\varepsilon} = \sqrt{\left(\frac{2}{3}\varepsilon_{ij}\varepsilon_{ij}\right)} \tag{5}$$

Where ε_{ij} is the strain rate tensor, defined as [23]:

$$\varepsilon_{ij} = \frac{1}{2}\left(\frac{\partial u_i}{\partial x_j} + \frac{\partial u_j}{\partial x_i}\right) \tag{6}$$

According to the materials physical changes during hot working, achieve the relation with mechanical and thermal properties during FSW in simulation procedure is necessary. Based on this factor, the PC alloy C_P, and K parameters are defined in Figure 1.Similarly, for Tungsten [23]:

$$C_p = 158 - 0.106T - 1.63\times10^{-5}T^2 \tag{7}$$

$$K = 0.367 - 2.29\times10^{-4}T + 1.25\times10^{-7}T^2 \tag{8}$$

The pressure field was obtained by solving the following continuity equation iteratively with the momentum equations for incompressible single-phase flow [23]:

$$\frac{\partial v_i}{\partial x_i} = 0 \tag{9}$$

that v_i is the velocity of plastic flow. The steady single-phase momentum conservation equations regarding a coordinate system attached to the heat source may be represented as [22]:

$$\rho C_p \frac{\partial (u_i T)}{\partial x_1} = -\rho C_p U_1 \frac{\partial T}{\partial x_1} + \frac{\partial}{\partial x_i}\left(k\frac{\partial T}{\partial x_i}\right) + Q_i + Q_b \tag{10}$$

The heat generated at the interface between vertical and horizontal surfaces of the tool pin and the workpiece may be defined as [22]:

$$Q_i = \left[(1-\delta)\eta\tau + \delta\mu_f P_N\right](\omega r - U_1 \sin\theta)\frac{A_r}{V} \tag{11}$$

where A_r is any small area on the tool pin-work piece interface, r is the radial distance of the center of the area from the tool axis, V is the control volume enclosing the area A_r, s is the maximum shear stress at yielding, θ is the angle with the negative x-axis in the counter-clockwise direction, η is the mechanical efficiency (the amount of mechanical energy converted to heat energy), δ denotes the spatially variable fractional slip between the tool and the workpiece interface, lf is the spatially variable coefficient of friction, ω is the angular velocity, and PN is the normal pressure on the surface.
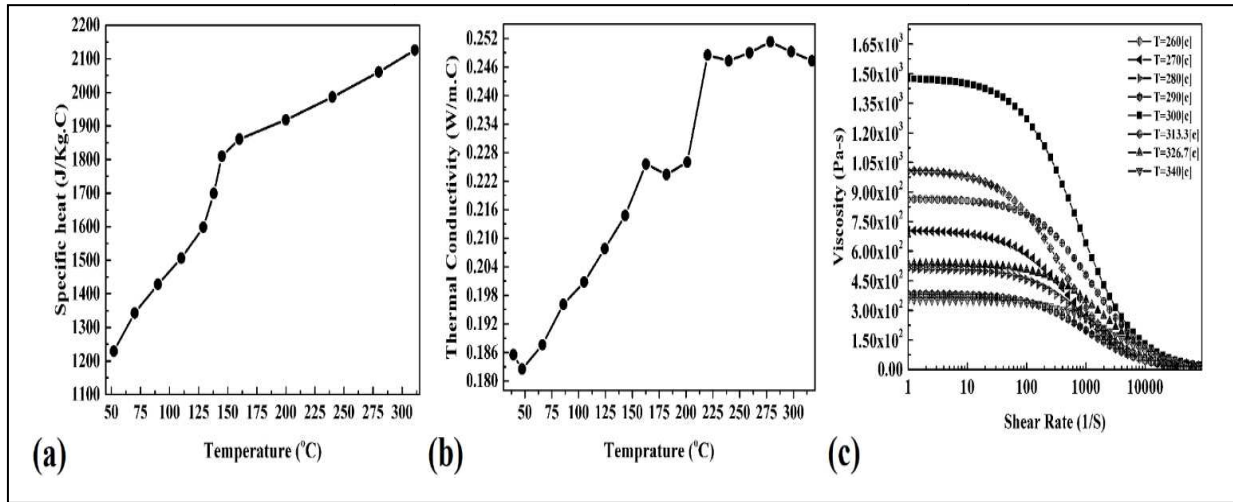

Figure1. (a) Specific heat, (b) Thermal conductivity, and (c) shear rate of PC

An estimate of the viscous dissipation of momentum per unit volume, Q_b, has been calculated as [23]:

$$Q_b = \frac{d\dot{\varepsilon}_p}{dV} = \beta\mu\varphi \tag{12}$$

Which φ is given by [23]:

$$\varphi = 2\sum_{i=1}^{3}\left(\frac{\partial u_i}{\partial x_i}\right)^2 + \left(\frac{\partial u_1}{\partial x_2}+\frac{\partial u_2}{\partial x_1}\right)^2 + \left(\frac{\partial u_1}{\partial x_3}+\frac{\partial u_3}{\partial x_1}\right)^2 + \left(\frac{\partial u_3}{\partial x_2}+\frac{\partial u_2}{\partial x_3}\right)^2 \tag{13}$$

In Equation (14), β is an arbitrary constant that indicates the extent of mixing on the atomic scale. The value of μ may tend to 1for a well-mixed system in the molecular scale [23]. The total heat generated at the shoulder/workpiece interface has been partitioned between the workpiece and the tool in the ratio given below [24- 25]:

$$q = \frac{\left(\sqrt{k\rho C_p}\right)_{workpiece}}{\left(\sqrt{k\rho C_p}\right)_{workpiece} + \left(\sqrt{k\rho C_p}\right)_{tool}} \tag{14}$$

Where the subscripts W and T denote the workpiece and the tool, respectively. The analytical expression is based on steady-state one-dimensional heat transfer from a point heat source located at the interface of dissimilar metals. The heat flux into the workpiece is estimated to be 45% of the total heat generated. This relation has been examined experimentally by Lienert et al. [26] and found to be reliable. A heat flux continuity at the shoulder matrix interface yields [22]:

$$k\frac{\partial T}{\partial Z}\bigg|_{Top} = \frac{J_w}{J_w + J_T}q_1 \tag{15}$$

R_P and R_S represent the tool pin and shoulder radius, respectively and q1 represents the total rate of heat generation at the shoulder–workpiece interface. It is given by [22]:

$$q_1 = \left[\eta(1-\delta)\tau + \delta\mu_F P_H\right](\omega r - U_1\sin\theta) \tag{16}$$

At the bottom surface, there is a backing plate and the heat transfer coefficient from the bottom of the workpiece is not the same as for free convection. The value of the heat transfer at the bottom of the workpiece was determined by:

$$k\frac{\partial T}{\partial Z}\bigg|_{Bottom} = h_b(T - T_a) \tag{17}$$

Where h_b is the bottom heat transfer coefficient and Ta is the ambient temperature of 298 K. The heat transfer coefficient at the bottom face depends on the local temperature and is given by the following relation:

$$h_b = h_{b0}(T - T_a)^{0.25} \tag{18}$$

Where h_{b0} is the heat transfer parameter for the bottom surface. As Equation (18) shows, this parameter is a constant and it has a different unit compared tothe heat transfer coefficient which is spatially variable. At the top surface, heat transfer is due to both convection and radiation and is given by:

$$-k\frac{\partial T}{\partial Z}\bigg|_{Top} = B_\varepsilon(T^4 - T_a^4) + h_t(T - T_a) \tag{19}$$

B is the Stefan–Boltzmann constant (5.67×10^{-16} J.K^{-4}.m^{-2}.s^{-1}), ε is the emissivity, and h_t is the convective heat transfer coefficient at the top surface. The computed temperature values were found to be insensitive to the values of h_t and its value was taken as zero for simplicity. During the simulation, the linear and rotational speed of the tool pin and shoulder were performed separately. The base metal assumed as non-Newtonian fluid with visco-plastic behaviour and density based on

PC. The Tetrahedral/Hybrid elements with T-grid combination shape were used to the mesh generation of tool and workpiece. The region close to the pin tool and the tool itself required a much finer mesh to evaluate the heat transfer model and viscous flow. A sizing function on the tool and workpiece was used to generate the different volume sizes. The sizing function uses a start size, growth rate, and maximum size. For the fine mesh pictured in Figure 2, a start size was 0.1 mm, growth rate 1.3 mm, and a maximum size of 1.3 mm. For this meshing scheme, the total number of volumes for the lateral case was 2,243,120 volumes.

3. Experimental Procedure

Friction Stir Welding experiments were conducted on polycarbonate (PC) sheets with 4 mm thickness supplied by Arkema Polymer Industry, USA. The sheet was cut into rectangles shape (100×150mm) by a laser cutting machine. Table 1 summarizes the main physical and mechanical properties of the PC sheet.A modified TABRIZ/4301 milling machine was used to perform the experimental tests. HSS steel made tool with a frustum pin profile was adopted in the experiments. Thermal histories were acquired at given locations using J-type thermocouple (Omega Engineering, USA).
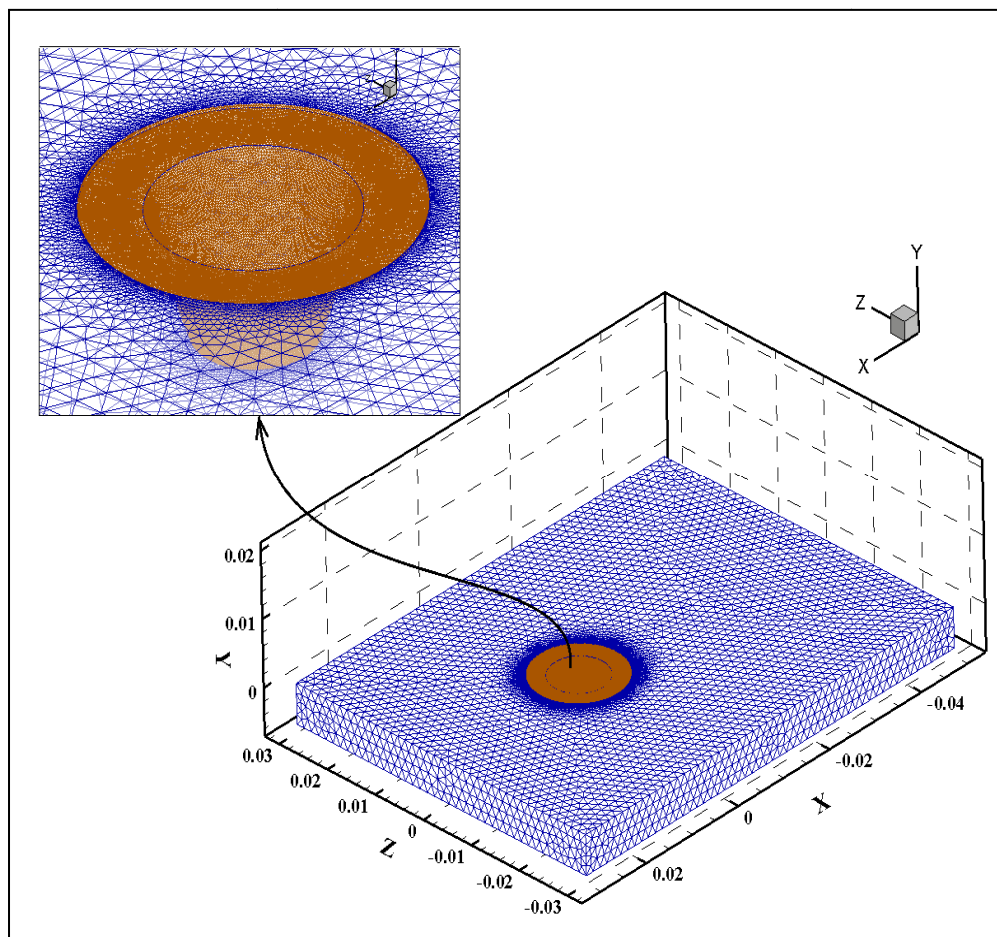

Figure2. Meshed model of the process

Table1. Properties of PC

Characteristics	Value
Density [g/cm^3]	1.22
Ultimate Tensile Strength [MPa]	67
Elongation at fracture [%]	98
Shear Stress [MPa]	101
Flexural Strength [MPa]	80
Hardness (ShoreD)	90
Charpy Notched Impact Strength [kJ/m^2]	25.2
Glass transition temperature, Tg [°C]	147
Thermal conductivity at 25°C [W/m·K]	0.22
Softening temperature [C]	225

The thermocouple, which was characterized by a 0.5 mm diameter, was embedded into the polycarbonate sheets at different distances (d=5, 10, and 15 mm) from the weld seam. To this end, holes were drilled at given locations and Testor's cement was used to bond the thermocouple inside the holes. Different characterization tests were performed on the welded specimens. A servo-controlled universal testing machine (SANTAM, Co. Tehran, Iran) with a load cell of 200 kN was adopted for quasi-static tests. Tensile and bending tests were conducted ata constant speed of 1 mm/min. The tensile tests were conducted according to the ASTM D638 standard. The notched IZOD impact tests were carried out according to the ASTM D256 standard. Material flow analyses have been carried out using a video visual measurement machine (MUMA, 3D Family, Xinbei City, Taiwan). A schematic of the FSW system is reported in Figure 3 with the FSW tool and mechanical testing samples. The experimental plan involved the variation of different process parameters including the tool rotation speed (ω), the welding speed (V), the tool plunge depth, and tilt angle. Table 1 summarizes the levels varied among the experiments and simulations.

Table2. FSW Parameters

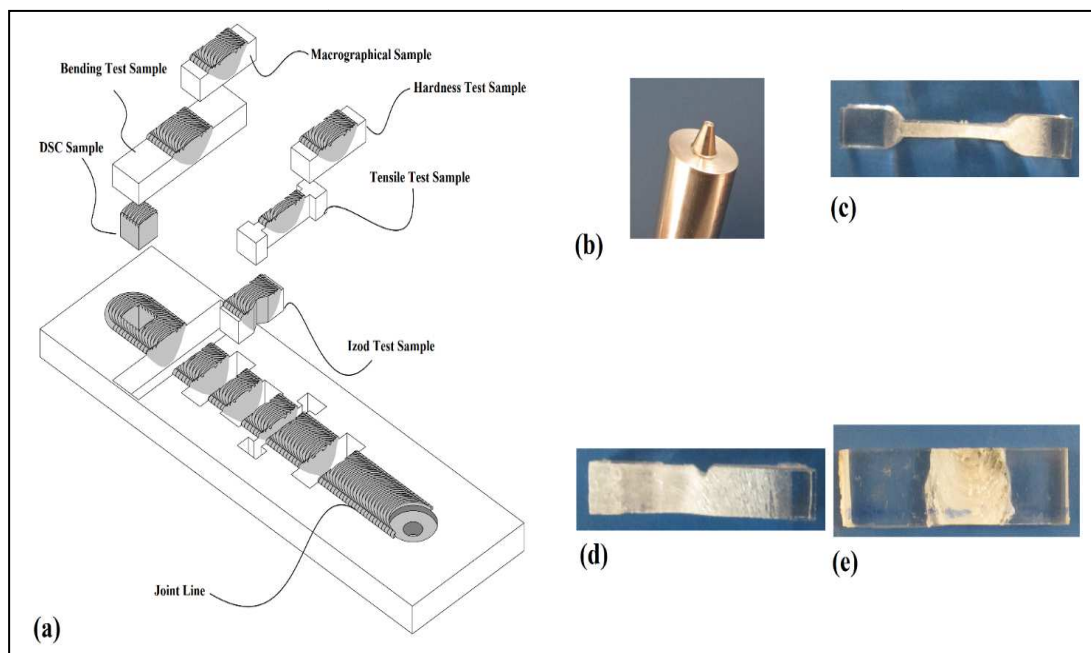| Process parameters	Value
ω [rpm]	2200
V [mm/min]	105
TPD [mm]	0.3, 0.6, 0.9, 1.2, 1.5, 1.8
α [degree]	0.5, 1.0, 1.5, 2.0, 2.5, 3.0, 3.5, 4.0

Figure3. (a) Schematic view of FSWed joint,(b) an electronic image of FSW tool,(c) tensile test sample,(d) Izod test sample,(e) flexural test sample

4. Results and Discussions

4.1 Material Flow

The tool plunge depth (TPD) influences the amount of frictional heat generated and the friction mechanism between the tool and sheets (i.e. sliding and sticking). This is also due to the increase in the axial force at the tool-sheets interface [24-25]. Figures 4(a) and 4(b) compare the temperature maps predicted by simulations involving the highest and the lowest tool plunge depth. Increasing the TPD from 0.3 mm to TDP=1.8 mm resulted in a higher maximum temperature from 194°C till 215°C. A low contact area between pin and PC and low heat transfer confident of PC caused slow heat diffusion of frictional heat from the upper area (that produced with tool shoulder) into the lower area of the stir zone. These thermal properties of PC caused little changes in the size of the SZ lower area at all TPD. But at higher TPDs, the material flow of the top surface joints changes. Physical changes of TPD effects can be detectable on Figures 4(c) and 4(d), respectively. According to the results, at low TPD the size of SZ decreases and at excessive TPD the big flash forms at AS which causes the formation of incomplete SZ. The dimension of the SZ is not monotonic with the tool plunge depth. Indeed, SZ increases with TPD until TPD≤1.2mm. Higher values of TDP determine a steep decrease in the SZ dimension. This is due to the formation of material ejected from the weld seam (which formed side flash). The comparison of recorded and simulated maximum temperature and size of SZ is shown in Figure 4. The positive tilt angle increases the plunging force and improves the material flow. It promotes the motion of the material from the front to the backside of the tool leading to a better filling of the stir zone [26-28].
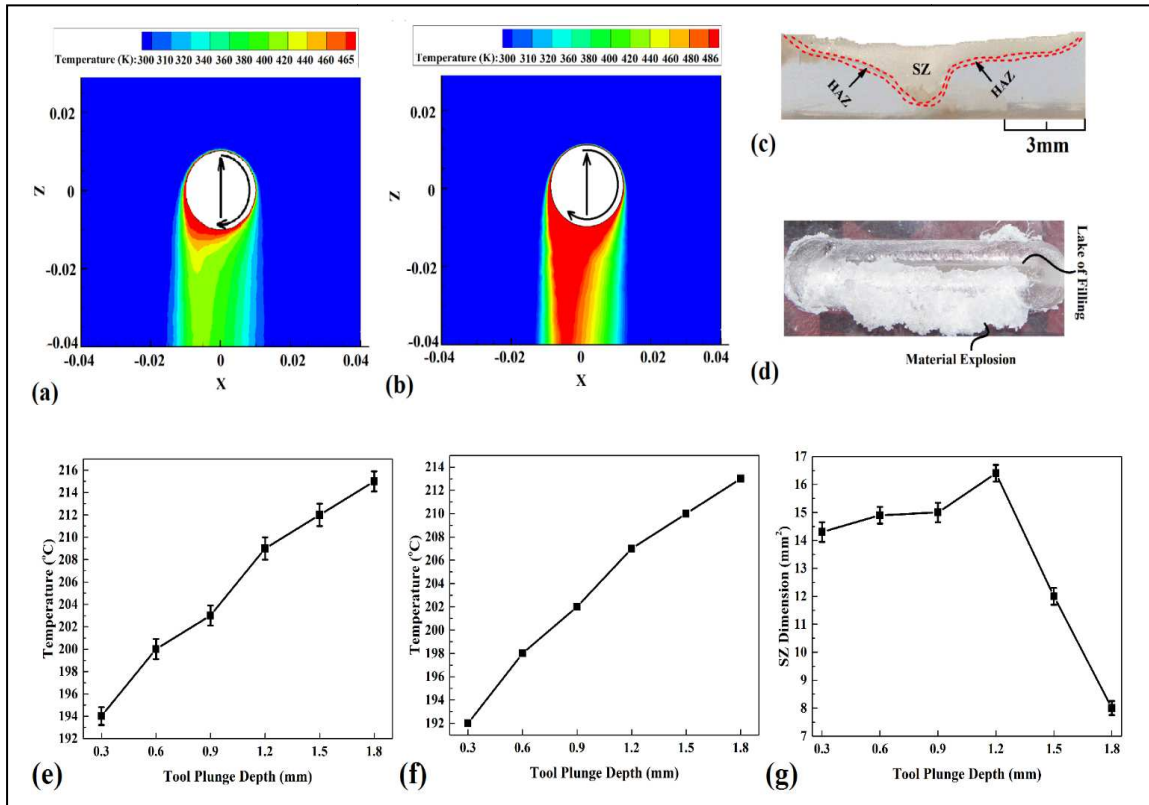
Figure4. Simulation results of surface heat flux of joint that FSWed at (a) 0.3mm and (b) 1.8mm TPD. (c) Cross-section view of the joint that FSWed at 0.3mm TPD and (d) surface flow of the joint that FSWed at 1.8mm TPD. Maximum temperature of FSWed joints at different TPD which (e) recorded and (f) simulated. (g) Relation with the size of SZ and TPD

This parameter also influences the heat produced. The temperature distributions simulated for different tilt angles in SZ are depicted in Figures 5(a)-5(c). The simulation indicates that an increase of α from 0.5^{o} to 4° degrees causes an increase of the maximum temperature by almost 17% (185°C from $\alpha=0.5^{o}$ till 215°C at $\alpha=4^{o}$). The maximum temperature was observed in correspondence of the behind the tool. Low values of α involved lower plunging load. This partially inhibits the material in front of the tool to extrude at the backside leading to defect development into the SZ.
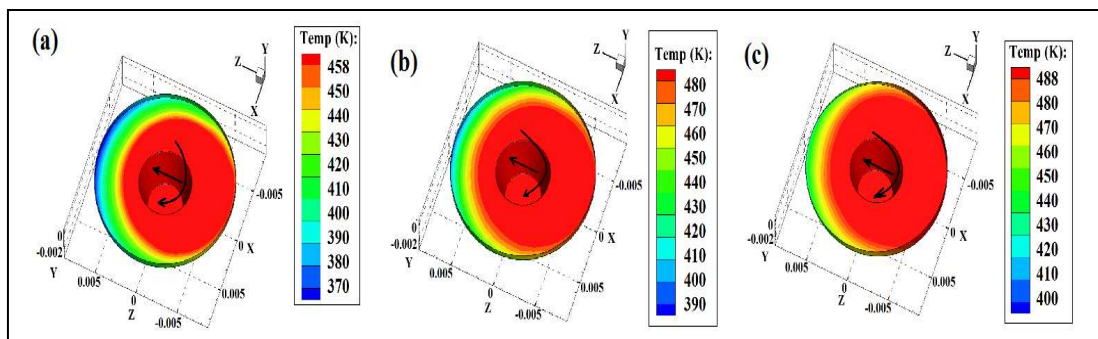

Figure5. Simulation results of maximum temperature at (a) 0.5, (b) 2 and (c) 4 degrees TTA

The longitudinal section of welds made with $\alpha=0.5^o$ and $\alpha=4^o$ tilt are shown in Figure 6. The temperature maps indicate that the temperature of the upper "layers" is much higher than that of the lower "layers" behind the SZ. The upper "layer" interacts with the tool shoulder that is much larger than the pin. On the upper side, the tool has a higher peripheral speed and interacts with the material for a longer time. Both these aspects contribute to increasing the temperature differences between the upper and lower "layers". The low heat generation in the lower area "layers" of SZ leads to the formation of the tunnel into the SZ root (Figure 6c). High values of α also resulted in the incomplete formation of the SZ (Figure 6d). The cross-sections reveal that similar tunnel voids are produced for low and high values of α.
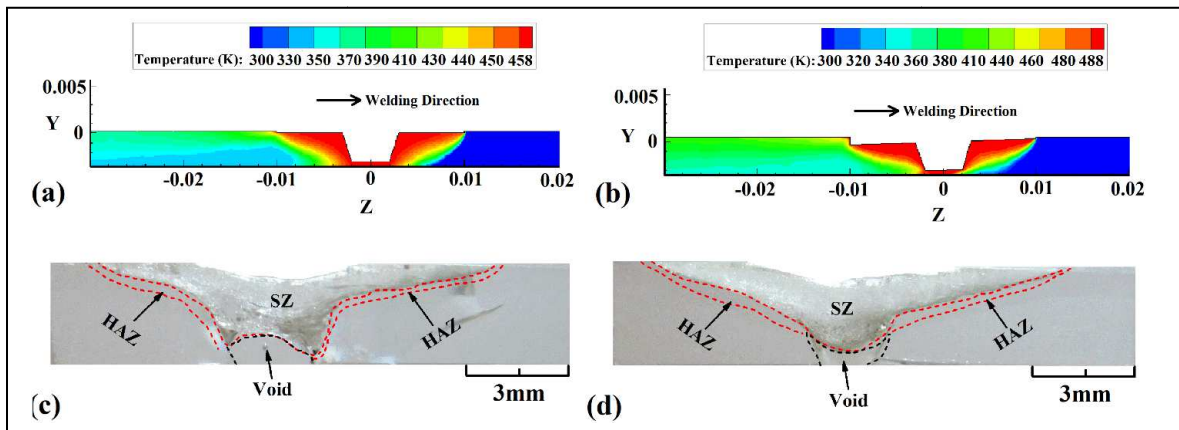

Figure6. Simulation results of longitudinal of maximum temperature flux at (a) 0.5, (b) 2 degrees TTA Cross-section view of joints that FSWed at (c) 0.5, (d) 2 degrees TTA

The welds produced with $\alpha=0.5°$ and $\alpha=4°$ showed a different morphology of the SZ. The former ones were characterized by an SZ with a convex shape of the root. On the other hand, the welds made with $\alpha=4°$ were characterized by a concave shape at the base of the weld root. The morphology of the welds revealed that increasing the value of α produced an increase in the maximum temperature of the process. Also, it increased the dimension of the SZ for $\alpha \leq 2.5°$. Further increase of α resulted in a steep decrease in the SZ dimension. This was due to the great amount of material ejected from the weld seam (Figure 7).
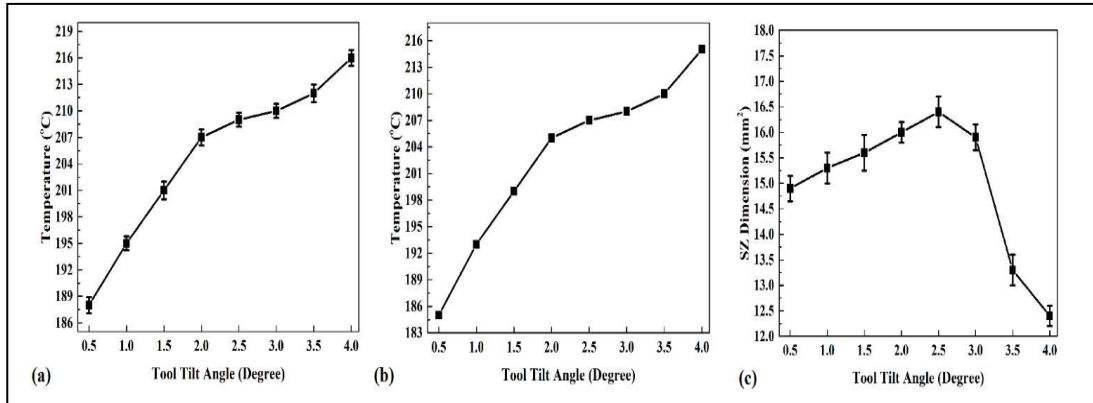
Figure7. Maximum temperature of FSWed joints at different TTA which (a) recorded and (b) simulated (c) Relation with the size of SZ and TTA

4.2 Mechanical Properties of Joint

4.2.1 Tensile Strength

The result indicates that processing conditions involving excessive heat input resulted in welds with lower strength. On the other hand, processing conditions involving low heat input were affected by the development of planar cracks around SZ. This determined the decrease of the tensile strength for low tool rotation and high travelling speeds. The highest tensile strength of the welds was 62MPa that was near 92% of the base material. Low values of TPD produced a poor material stirring, while high TPD values induced a great amount of material ejected from the SZ. Both these defects affected the mechanical behaviour of the welds; thus, the highest strength was achieved at intermediate values of TPD=1.2mm. Similarly, the highest strength was achieved for $\alpha=2.5°$ (Figure 8). The fracture surface of the strongest joint is depicted in Figure 8c. The surface is rough and shows divergent lines. These lines radiating outward from the fracture origin are called "hackled regions". Hackled regions show the crack propagation direction and point back toward the origin area [27-29]. Hackles lines are very similar to river lines that appear in the fracture surface of metallic materials [29-30].
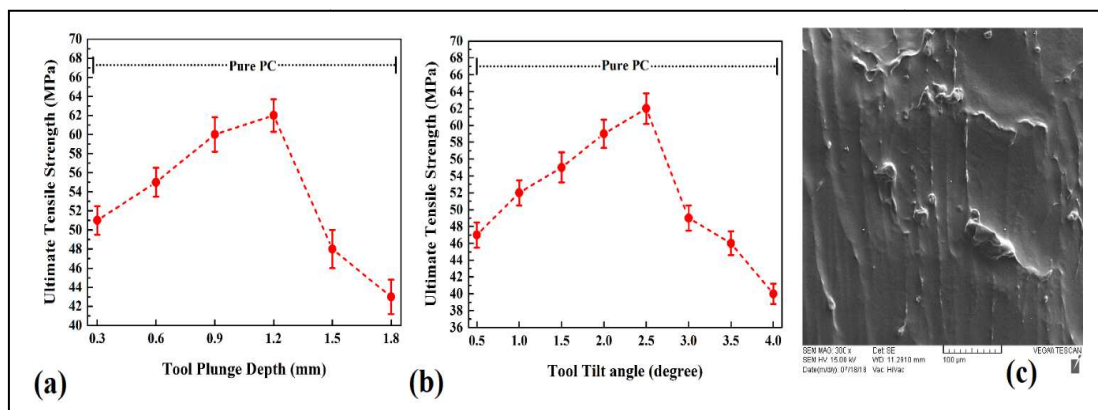

Figure8. Relation with tensile strength and (a) TPD and (b) TTA (c) SEM image of the fracture surface of the joint that FSWed 2°TTA and 1.2 TPD

4.2.2 Flexural Test

Figure 9 summarizes the effect of the process parameters on the flexural strength. The trend of the flexural strength follows those of the tensile strength. Under the optimal processing conditions, the flexural strength reaches 71MPa, which almost 89% of that of the base material. The fracture surfaces of the weld produced under the aforementioned conditions are shown in Figure 9c. The state of flexural stress mode causes the formation of crack branches. This type of fracture surface is typical of transparent polymers such as polystyrene, poly (methyl methacrylate), and polycarbonate are shown bifurcations crack path move away from crack origins. This type of cracks branches is observed at the fracture surface in the flexural test specimens due to the state of stress during bending.
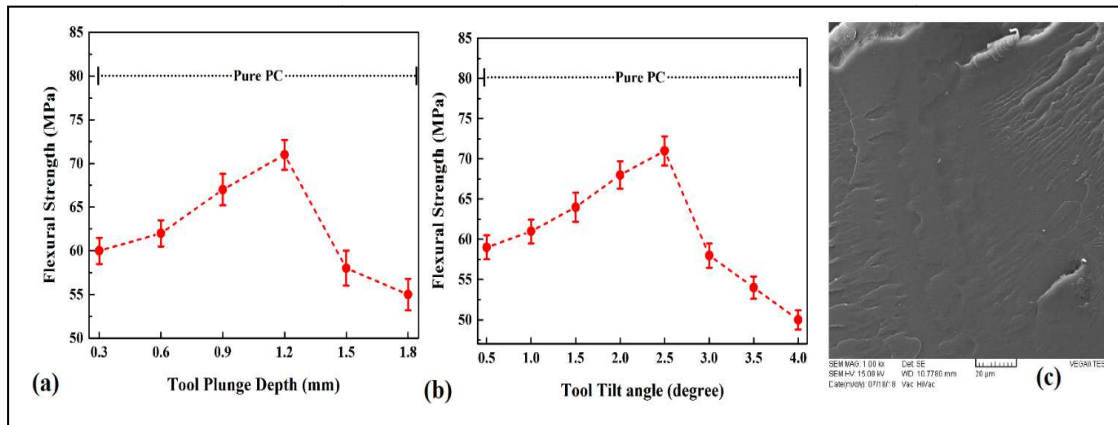

Figure9. Relation with flexural strength and (a) TPD and (b) TTA, (c) SEM image of the fracture surface of the joint that FSWed 2°TTA and 1.2 TPD

4.2.3 Izod Test

Figure 10 shows the Izod test sample of the FSWed PC. The processing conditions leading to the highest tensile and flexural strength also resulted in the highest impact energy absorbed by the welds. Under these conditions, the weld absorbed 22 kJ/m2, which is almost 86% of the impact strength of the PC. The fracture surfaces of the weld produced under the optimal conditions (ω=2200 rpm, V=105mm/min, α=2.5° TTA and TPD=1.2mm). The surface shows a misty appearance that can be associated with crack acceleration just before rapid crack growth during the Izod test.

5. Conclusion

The effects of FSW processing conditions including tool title angle and plunge depth on the mechanical strength and material flow of polycarbonate were studied. Thermo mechanical models were employed to predict the temperature profile along with the transverse and longitudinal directions.The surface temperature was also experimentally measured and compared with simulations. The most appropriate material flow and joint strength were achieved at 1.2 mm plunge depth. The joints which were welded at more than 1.2 mm plunge depth had inappropriate internal material flow while small stir zone was formed at a lower 1.2 mm tool plunge depth. At high tool tilt angle, the increased forging force within the plastic material led to material explosion formation

of defects, while a lower tool tilt angle does not extrude the material to form a complete stir zone. A tilt angle of 2.5o was also found preferable to obtain sound weldments with improved strength. The highest tensile strength (62MPa), flexural strength (71MPa), and impact energy (22 kJ/m2) were attained for joints processed at 2.5o tilt angle, 1.2 mm plunge depth, 105 mm/min traverse speed, and 2200 rpm tool rotational speed.
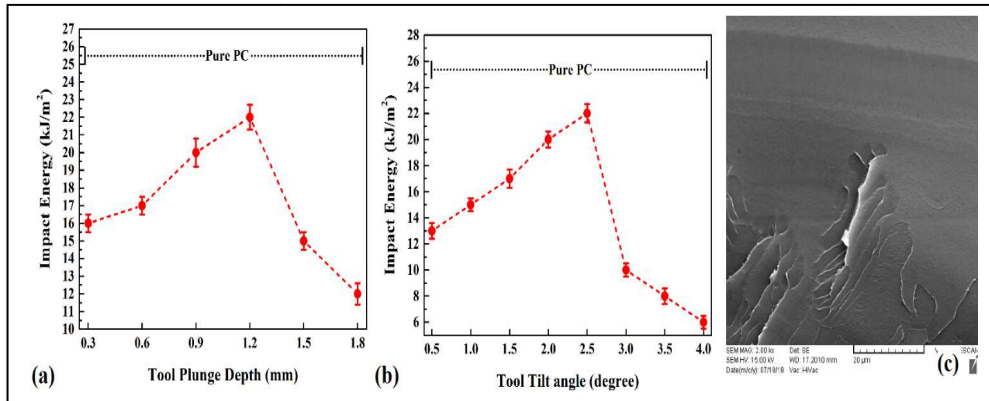

Figure10. Relation with impact energy and (a) TPD and (b) TTA, (c) SEM image of the fracture surface of the joint that FSWed 2°TTA and 1.2 TPD

6. References

[1] Aghajani Derazkola, H., Habibnia, M. and Jamshidi Aval, H. 2015. Study on Frictional Heat Behavior and Material Flow during Friction Stir Welding of AA1100 Aluminum Alloy. Modares Mechanical Engineering. 14: 251-261.

[2] Elyasi, M., Aghajani Derazkola, H. and Hosseinzadeh, M. 2015. Effects of friction stir welding parameters on mechanical quality of AA1100 aluminum alloy to A441 AISI steel joint. Modares Mechanical Engineering. 15: 379-390.

[3] Aghajani Derazkola, H., Elyasi, M. and Hosseinzadeh, M. 2016. Effects of friction stir welding tool plunge depth on microstructure and texture evolution of AA1100 to A441 AISI joint. International Journal of Advanced Design and Manufacturing Technology. 9: 13-20.

[4] Aghajani Derazkola, H., Elyasi, M. and Hosseinzadeh, M. 2015.Formation of defects and intermetallic compounds in friction stir welding of AA1100 alloy to A441 AISI steel. Advanced processes in materials. 9(3): 219-233.

[5] Elyasi, M., Aghajanai Derazkola, H. and Hosseinzadeh, M. 2016. Investigations of tool tilt angle on properties friction stir welding of A441 AISI to AA1100 aluminium, Proceedings of the Institution of Mechanical Engineers, Part B: Journal of Engineering Manufacture. 230(7): 1234-1241.

[6] Aghajanai Derazkola, H. and Simchi, A. 2018. Effects of Alumina Nanoparticles on the Microstructure, Strength and Wear Resistance of Poly (Methyl Methacrylate)-based Nanocomposites Prepared by Friction Stir Processing. Journal of the Mechanical Behavior of Biomedical Materials. 79: 246-253.

[7] Elyasi, M., Aghajanai Derazkola, H. and Hosseinzadeh, M. 2015. Study on joint zone microstructure evolution and hardness in friction stir welding of AA1100 aluminum alloy to A441 AISI steel. Modares Mechanical Engineering. 14: 97-107.

[8]Aghajani Derazkola, H., Elyasi, M. and Hosseinzadeh, M. 2014. Feasibility Study on Aluminum Alloys and A441 AISI Steel Joints by Friction Stir Welding. International Journal of Advanced Design and Manufacturing Technology.7: 99-109.

[9] Mironov, S., Sato, S. Y. and Kokawa H. 2018.Friction-stir welding and processing of Ti-6Al-4V titanium alloy: A review.Journal of Materials Science and Technology. 34(1): 58-72.

[10] Smith, C., Bendzsak, G., North, T., Hinrichs, J., Noruk, J. and Heideman, R. 1999. Heat and Material Flow Modeling of the Friction Stir Welding Process. 11th International Conference on Computer Technology in Welding, Detroit. United State.

[11] Arici, A. and Selale, S. 2007.Effects of tool tilt angle on tensile strength and fracture locations of friction stir welding of polyethylene. Science and Technology of Welding and Joining. 12: 536-539.

[12] Aydin, M. 2010.Effects of welding parameters and pre-heating on the friction stir welding of UHMW-polyethylene. Polymer-Plastics Technology and Engineering. 49: 595-601.

[13] Saeedy, S. and BesharatiGivi, M.K. 2011. Investigation of the effects of critical process parameters of friction stir welding of polyethylene. Journal of Engineering Manufacture, Proceedings of the Institution of Mechanical Engineers Part B. 225(8): 1305-1310.

[14] Panneerselvam, K. and Lenin, K. 2013. Lenin Effects and defects of the polypropylene plate for different parameters in friction stir welding process. International Journal of Renewable Energy Technology. 2(2): 143-152.

[15] Panneerselvam, K. and Lenin, K. 2014. Joining of Nylon 6 plate by friction stir welding process using threaded pin profile. Materials & Design. 53: 302-307.

[16] Aghajanai Derazkola, H. and Simchi, A. 2018. Experimental and thermomechanical analysis of the effect of tool pin profile on the friction stir welding of poly (methyl methacrylate) sheets. Journal of Manufacturing Processes. 34(A): 412-423.

[17] Elyasi, M. and Aghajanai Derazkola, H. 2018.Experimental and Thermomechanical Study on FSW of PMMA Polymer T-joint. International Journal of Advanced Manufacturing Technology. 98(1-4): 1445-1456.

[18] Aghajanai Derazkola, H., Simchi, A. and Lambiase, F. 2019. Friction Stir Welding of Polycarbonate Lap Joints: Relationship between Processing Parameters and Mechanical Properties. Polymer Testing. 79: 105999.

[19] Aghajanai Derazkola, H. and Simchi, A. 2018. Experimental and Thermomechanical Analysis of Friction Stir Welding of Poly (Methyl Methacrylate) Sheets. Science and Technology of Welding and Joining. 23(3): 209-218.

[20] Aghajani Derazkola, H. 2017. Effects of tool linear and rotational speed on material flow and heat generation of poly methyl methacrylate (PMMA) friction stir welding. Journal of Simulation and Analysis of Novel Technologies in Mechanical Engineering. 9(4): 687-700.

[21] Aghajani Derazkola, H. and Khodabakhshi, F. 2019. Intermetallic compounds (IMCs) formation during dissimilar friction-stir welding of AA5005 aluminum alloy to St-52 steel: numerical modeling and experimental study. International Journal of Advanced Manufacturing Technology. 100(9-12): 2401-2422.

[22] Aghajani Derazkola, H. and Jamshidi Aval, H. 2015. Study on heat generation and distribution during friction stir welding of AA1100 aluminum alloy. International Journal of Advanced Design and Manufacturing Technology. 8: 9-17.

[23] Aghajani Derazkola, H., Elyasi, M. and Hosseinzadeh, M. 2015. CFD Modeling of Friction Stir Welding of AA1100 Aluminum Alloy to A441 AISI Steel Butt Joint. Journal of Advanced Materials and Processing. 3(3): 47–59.

[24] Aghajani Derazkola, H., Khodabakhshi, F. and Simchi, A. 2018. Friction-stir lap-joining of aluminium-magnesium/poly-methyl-methacrylate hybrid structures: thermo-mechanical modelling and experimental feasibility study. Science and Technology of Welding and Joining. 23(1): 35-49.

[25] Aghajani Derazkola, Kashiry Fard, R. H. and Khodabakhshi, F. 2018. Effects of processing parameters on the characteristics of dissimilar friction-stir-welded joints between AA5058 aluminum alloy and PMMA polymer. Welding in the World. 62(1): 117-130.

[26] Aghajani Derazkola, H. and Khodabakhshi, F. 2019. A novel fed friction-stir (FFS) technology for nanocomposite joining. Science and Technology of Welding and Joining. https://doi.org/10.1080/13621718.2019.1631534.

[27] Aghajani Derazkola, H. and Khodabakhshi, F. 2019.Underwater submerged dissimilar friction-stir welding of AA5083 aluminum alloy and A441 AISI steel. International Journal of Advanced Manufacturing Technology. 102(9-12): 4383-4395.

[28] Aghajani Derazkola, H. and Simchi, A. 2019. An investigation on the dissimilar friction stir welding of T-joints between AA5754 aluminum alloy and poly (methyl methacrylate). Thin-Walled Structures. 135: 376-384.

[29] Aghajanai Derazkola, H. and Elyasi, M. 2018. The influence of process parameters in friction stir welding of Al-Mg alloy and polycarbonate. Journal of Manufacturing Processes. 35: 88-98.

[30] Aghajani Derazkola, H. 2017. Simulation of Tool Rotation and Travelling Speed Effects on Friction Stir Welding of Ti-6Al-4V. Journal of Modern Processes in Manufacturing and Production. 6(4): 81-98.